

Article

Preparation of Palladium Nanoparticles Decorated Polyethyleneimine/Polycaprolactone Composite Fibers Constructed by Electrospinning with Highly Efficient and Recyclable Catalytic Performances

Cuiru Wang ^{1,2}, Juanjuan Yin ², Shiqi Han ², Tifeng Jiao ^{1,2,*} , Zhenhua Bai ³, Jingxin Zhou ², Lexin Zhang ² and Qiuming Peng ^{1,*}

¹ State Key Laboratory of Metastable Materials Science and Technology, Yanshan University, Qinhuangdao 066004, China; wcr2016ysdx@163.com

² Hebei Key Laboratory of Applied Chemistry, School of Environmental and Chemical Engineering, Yanshan University, Qinhuangdao 066004, China; jjy1729@163.com (J.Y.); auslineus@163.com (S.H.); zhoujingxin@ysu.edu.cn (J.Z.); zhanglexin@ysu.edu.cn (L.Z.)

³ National Engineering Research Center for Equipment and Technology of Cold Strip Rolling, Yanshan University, Qinhuangdao 066004, China; bai_zhenhua@aliyun.com

* Correspondence: tfjiao@ysu.edu.cn (T.J.); pengqiuming@ysu.edu.cn (Q.P.); Tel.: +86-335-805-6854 (T.J.)

Received: 24 May 2019; Accepted: 21 June 2019; Published: 22 June 2019



Abstract: Nano-sized palladium nanoparticles showed high catalytic activity with severe limitations in catalytic field due to the tendency to aggregate. A solid substrate with large specific surface area is an ideal carrier for palladium nanoparticles. In present work, polyethyleneimine/polycaprolactone/Pd nanoparticles (PEI/PCL@PdNPs) composite catalysts were successfully designed and prepared by electrospinning and reduction methods using PEI/PCL electrospun fiber as carrier. The added PEI component effectively regulated the microscopic morphology of the PEI/PCL fibers, following a large number of pit structures which increased the specific surface area of the electrospun fibers and provided active sites for loading of the palladium particles. The obtained PEI/PCL@PdNPs catalysts for reductions of 4-nitrophenol (4-NP) and 2-nitroaniline (2-NA) exhibited extremely efficient, stable, and reusable catalytic performance. It was worth mentioning that the reaction rate constant of catalytic reduction of 4-NP was as high as 0.16597 s^{-1} . Therefore, we have developed a highly efficient catalyst with potential applications in the field of catalysis and water treatment.

Keywords: electrospinning; palladium nanoparticles; composite films; catalysis

1. Introduction

In recent years, there has been an increasing shortage of water sources available in the context of rapid technological and economic development, and widespread attention has been paid to the protection and purification of water sources. Harmful organic waste is a main source of water pollution. That conversion of harmful organic chemicals into harmless or low toxicity compounds under mild conditions has become an extremely important area of research. It is well known that 4-nitrophenol (4-NP) is widely used in the synthesis of dyes and medicines, and is one of the common chemical products used in the chemical industry [1]. However, it is prone to contaminate soil and water [2]. Methods for purifying such compounds are photocatalytic degradation [3], adsorption [4], microbial degradation [5], and nitro reduction [6], etc. Among these methods, the nitro reduction is one of the most commonly used methods and has the characteristics of simple process, mild conditions and environmental protection [7]. Therefore, it is important to develop effective catalysts to convert hazardous organics into reusable products.

Precious metal particles with excellent catalytic activity, such as palladium, have received extensive attention [8–10]. However, the palladium nanoparticles with small particle size and high surface energy are unstable and tend to agglomerate, inhibiting their catalytic activity and catalytic efficiency [11]. An effective way to solve the aggregation of metal particles is to load the particles on a carrier substrate [12–16]. Recently, several different palladium-based catalysts have been reported. Lebaschi et al. synthesized Pd@B.tea NPs catalyst which used environmentally friendly natural black tea extract as a reducing agent, was simple in preparation and excellent in catalytic performance [17]. Wu et al. synthesized CN-supported PdNPs nanocomposites using cellulose nanocrystals (CN) that acted as both supporting substrate and reducing agent, which exhibited higher catalytic activity in catalytic reduction of methylene blue and 4-NP [18]. Chen et al. prepared bimetallic AuPdNPs/GNs catalysts by one-pot method utilizing graphene nanosheets (GNs) with large specific surface area, which showed higher catalytic ability than single metal catalysts [19]. Le et al. reported the preparation of fibrous nano-silica supported palladium nanocatalyst (Pd/KCC-1), and the unique dendritic fiber morphology of the support (KCC-1) resulted in poor aggregation of palladium nanoparticles [20].

Electrospinning is a simple and effective method for the direct and continuous preparation of polymer nanofibers [21,22]. The prepared electrospun fibers have unique characteristics, such as specific surface area and high porosity [23,24], which can be widely used in the fields of adsorption [25,26], catalysis and filtration [27–30]. Therefore, electrospun fibers can be used as an ideal carrier for metal nanoparticles. Polycaprolactone (PCL) containing abundant polar methylene and ester groups has good biodegradability, biocompatibility and mechanical properties, which is one of the most easily used polymers for electrospinning [31–33]. However, the hydrophobicity of polycaprolactone fibers limits their application in water soluble systems. Polyethyleneimine (PEI) contains many amino functional groups, which are combined with PCL to improve the hydrophilicity of the fibers. In present work, based on the characteristic of large surface area of electrospinning fibers, PEI/PCL composite fibers were prepared as a carrier for supporting palladium nanoparticles, which provide active sites. The surface modification of the PEI/PCL fibers was achieved by changing the content of the PEI component, and the appearance of the pit structures further increased the specific surface area of the fibers and the active sites for supporting palladium particles. The catalytic reduction of 4-nitrophenol and 2-nitroaniline by PEI/PCL@PdNPs composite catalyst showed extremely high catalytic activity and stability, which meant potential application in water purification and catalysis.

2. Results and Discussion

2.1. Characterization of PEI/PCL@PdNPs Composites

Figure 1 illustrated the experimental process of electrospinning, chemical modification and catalytic reduction in the preparation and application of PEI/PCL@PdNPs composite catalyst. Firstly, the granular PCL and the liquid PEI were dissolved in a good organic solvent, chloroform, to obtain a homogeneous electrospinning precursor solution which was magnetically stirred at room temperature overnight. The precursor solution, placed in a 10 mL syringe with a stainless steel needle (20G), was electrospun under a high voltage driving force to obtain a PEI/PCL composite fiber. Secondly, NaBH₄ as a good reducing agent reduced aqueous PdCl₂ to palladium to obtain a solution containing palladium nanoparticles. The prepared PEI/PCL fibers were immersed in the palladium nanoparticles solution for one hour to complete chemical modification and obtained PEI/PCL@PdNPs composites. Finally, the prepared PEI/PCL@PdNPs was used as catalyst to catalytically reduce 4-NP and 2-NA to explore its catalytic activity. Due to the large number of functional groups present in PEI, it was possible that some NH₂ groups reacted with the carbonyl ester bond, and other functional amine groups remained free on the surface, allowing them to bind to other molecules such as palladium [34].

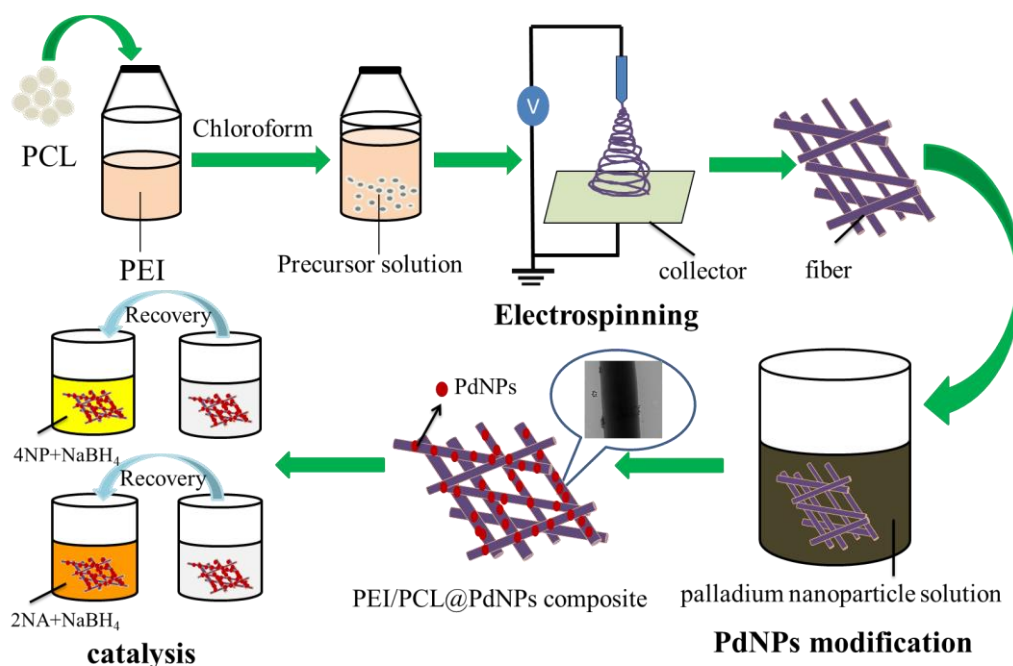


Figure 1. Preparation process of polyethyleneimine/polycaprolactone/Pd nanoparticles (PEI/PCL@PdNPs) composite and its catalytic performance.

Figure 2 depicted the scanning electron microscope (SEM) surface morphologies of PEI/PCL fibers (Samples 1–6) at different PEI contents. It was clear that the structures of the PEI/PCL electrospun fibers were related to the mixing ratio of PEI and PCL. PEI/PCL fibers of different mixing ratios exhibited inhomogeneous thickness structure. As the PEI content increased, the smooth PEI/PCL composite fibers gradually appeared pits on the fiber surface. The larger the mixing ratio of PEI to PCL, the more and deeper pits on the fiber surface. It was well known that parameters such as polymer viscosity and concentration were key factors influencing electrospinning [22]. The pit structure of the PEI/PCL electrospun fiber was attributed to the difference of PEI component contained in the polymer fibers. As shown in Table 1, the specific surface area of PEI/PCL fibers improved from 8.34 to 12.93 m²g⁻¹ with the increment of PEI component in composite fibers. The electrospun fibers with pit-like surface structures further increased the specific surface area of the fibers, which increased the particles attachment sites and helpful to next modification of palladium nanoparticles on surface of the synthesized composite fiber.

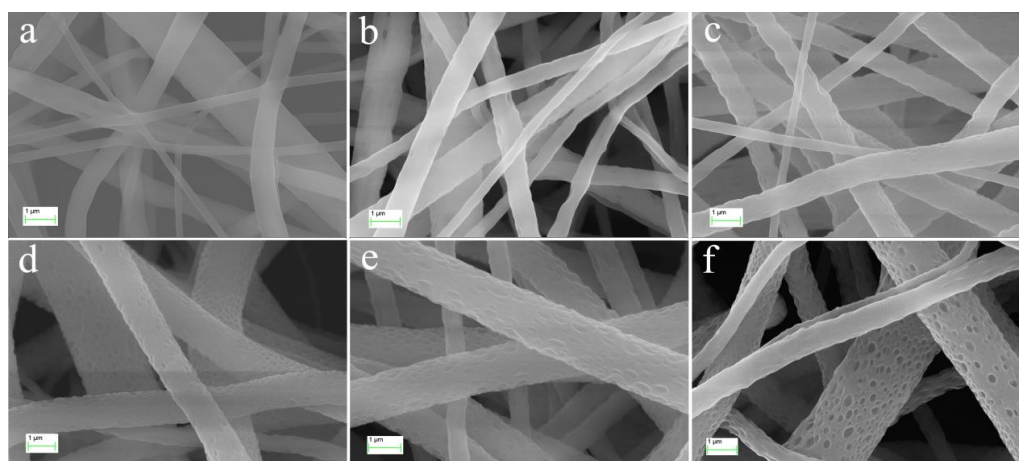


Figure 2. SEM images of AuNPs coated PEI/PCL electrospun fibers with different weight ratios ((w/w) (a), 10:90; (b), 15:85; (c), 20:80; (d), 25:75; (e), 30:70; (f), 35:65).

Table 1. Physical data of as-prepared different fiber composites.

PEI/PCL Fibers Samples of Different Weight Ratios	Specific Surface Area (m^2g^{-1})	Average Pore Diameter (nm)	Pore Volume (cm^3g^{-1})
10:90	8.34	23.83	0.00867
15:85	8.84	25.31	0.00919
20:80	9.73	27.86	0.01018
25:75	11.16	31.92	0.01144
30:70	11.82	33.56	0.01231
35:65	12.93	36.85	0.01322

In order to further observe the structure of as-prepared PEI/PCL@PdNPs composite, the transmission electron microscopy (TEM) morphologies of the obtained fibers were examined, as shown in Figure 3. It was obvious that the surface of PEI/PCL fiber (sample 6, w/w, 35:65) was uneven, as shown in Figure 3b. The rugged structure increased the specific surface area helpful to next chemical modification of the fibers. It could be seen in Figure 3c that the PdNPs modified on the surface of PEI/PCL fibers showed the mean size range of 5–10 nm. As shown in Figure 3d, the interplanar spacing of the palladium nanoparticles was 0.2243 nm, which well matched the (111) crystal plane of Pd [35]. Furthermore, the Pd element mapping shown in Figure 3e was good evidence of the presence and distribution of palladium nanoparticles on the surface of the prepared PEI/PCL fibers. It was reasonably speculated that hydrophilic PdNPs were successfully anchored on the surface of PEI/PCL composite fibers via weak intermolecular interactions, then the composites could be expected good catalytic activity in next catalytic process [36,37].

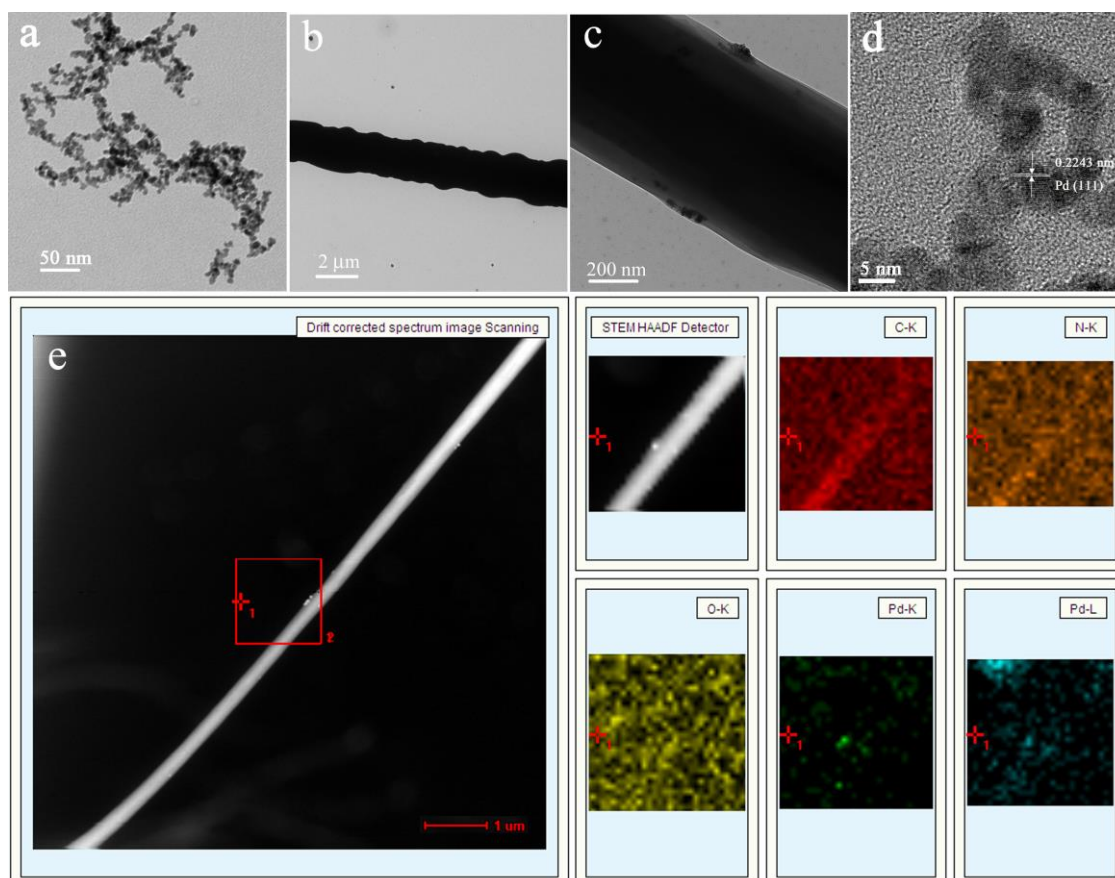


Figure 3. TEM images of the synthesized PdNPs (a), PEI/PCL fibers at 35:65 weight ratio (b) and modified with PdNPs (c), high resolution of PdNPs (d), and C/N/O/Pd elemental mapping (e) of PEI/PCL@PdNPs composites. The scale size of elemental mapping is 1.5 μm .

In addition, the morphology of PEI/PCL@PdNPs was characterized by scanning electron microscope (SEM), as shown in Figure 4. Figure 4a depicted the SEM structure of PEI/PCL@PdNPs, and it was apparent that deposits were present on the surface of the PEI/PCL fibers. The energy dispersive spectroscopy (EDS) image of the obtained PEI/PCL@PdNPs shown in Figure 4b–d clearly showed the presence of carbon, oxygen, nitrogen, and palladium elements. Due to the shielding effect, only a part of the nitrogen element in the PEI could be displayed, as shown in Figure 4d. The presence of small amounts of gold and copper was due to the coated-gold treatment and copper substrate used during the measurement. From EDS data, the detailed atomic percentages were found to be C = 75.37%, O = 12.61%, N = 7.88%, and Pd = 1.23%. The above results indicated that the palladium nanoparticles were successfully modified on the surface of the PEI/PCL fibers.

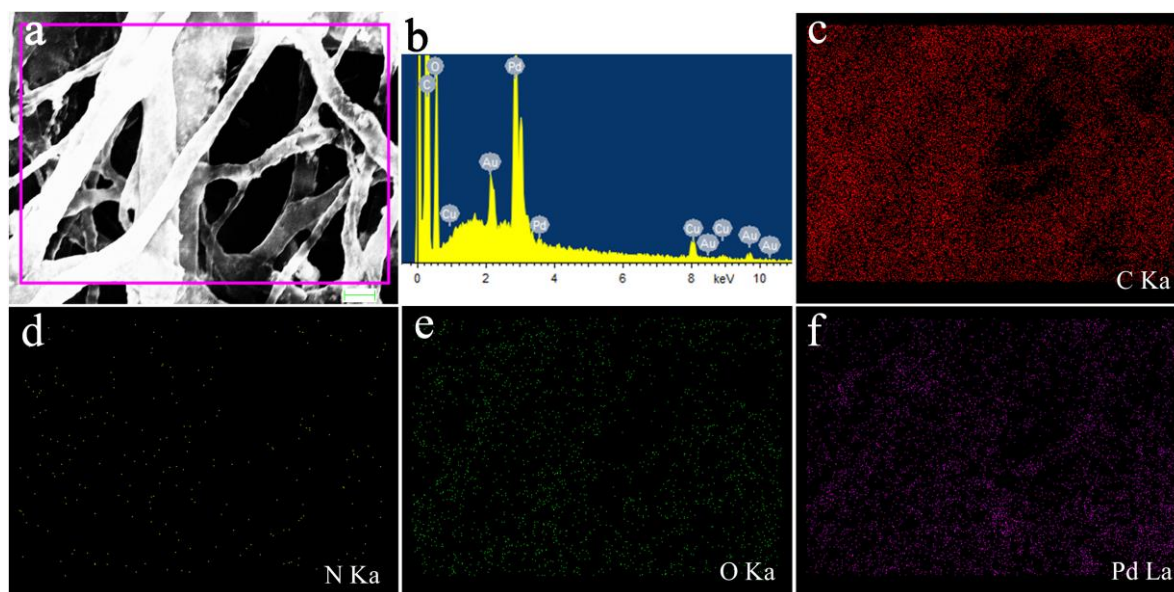


Figure 4. Scanning electron microscope (SEM) and EDS images of as-prepared PEI/PCL@PdNPs composite (a,b) and C/O/N/Pd elemental mapping (c–f). The scale bar in image a represent 1 μm .

The prepared PEI/PCL fibers and PEI/PCL@PdNPs composite were further characterized by X-ray diffraction spectroscopy, as shown in Figure 5. It was obvious from curves (a) and (b) that both the PEI/PCL composite fibers with different weight ratios showed characteristic diffraction peaks at $2\theta = 21.4^\circ$ and 23.8° . The PEI/PCL fiber with low PEI component showed strong characteristic peaks, while the binary fiber with high PEI component showed the weaker intensity of the characteristic peak. The difference in the intensity of the characteristic peaks of PEI/PCL fibers with different blend ratios demonstrated that the higher the PEI component, the lower the crystallinity of the composite fibers. From the X-ray diffraction spectrum of the PEI/PCL@PdNPs composite, it could be seen that a characteristic peak appeared at $2\theta = 40.1^\circ$, corresponding to the (111) crystal plane of the palladium particles, which further proved that the palladium nanoparticles successfully modified the PEI/PCL composite fibers [38,39]. In addition, the characteristic peak intensity of the PEI/PCL@PdNPs composite increased as the palladium particles were successfully modified on the surface of the PEI/PCL composite fibers.

To investigate the thermal stability of the prepared PEI/PCL@PdNPs composite, the thermogravimetric characterization of the obtained PCL fibers, PEI/PCL fibers, and PEI/PCL@PdNPs composite were measured under argon gas atmosphere, as shown in Figure 6. TG analysis of the three composite fiber materials showed that the weight loss was slower when the temperature was lower than 120°C due to the volatilization of residual moisture in the samples [40]. In addition, when the temperature was higher than 500°C , the quality of the three species of samples tended to be stable. Between 120°C and 450°C , the weight of above-mentioned three samples was firstly

slow loss, and then the weight of these samples was sharply lost at 400 °C, which was due to the thermal decomposition of various chemical groups and alkyl chains contained in these samples at high temperature [41]. The temperature points with mass loss 5 wt.% showed the values of 353, 311, and 236 °C for PCL fibers, PEI/PCL fibers, and PEI/PCL@PdNPs composite fibers, respectively, indicating that the addition of the PEI component and PdNPs reduced the thermal stability of the composite fibers. The above significant difference in the thermal stability could reasonably be attributed to the inclusion of palladium nanoparticles on the surface of the composite fibers.

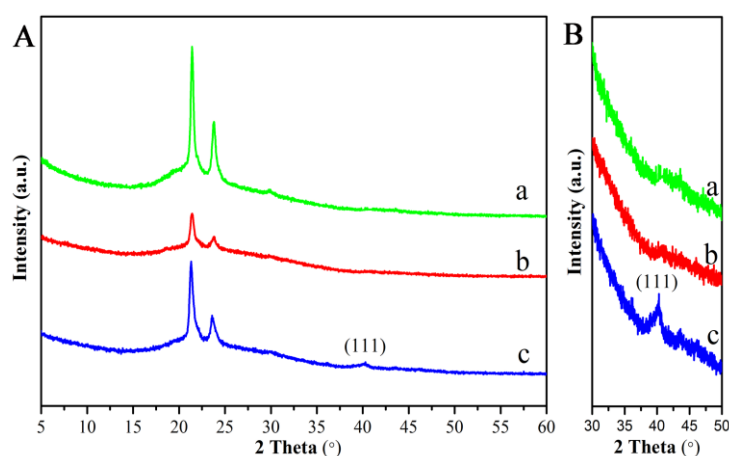


Figure 5. X-ray diffraction spectroscopy (XRD) pattern (A) with zoom-in region (B) of PEI/PCL fibers with the weight ratios of 10:90 (a) and 35:65 (b) and PEI/PCL@PdNPs composite (c).

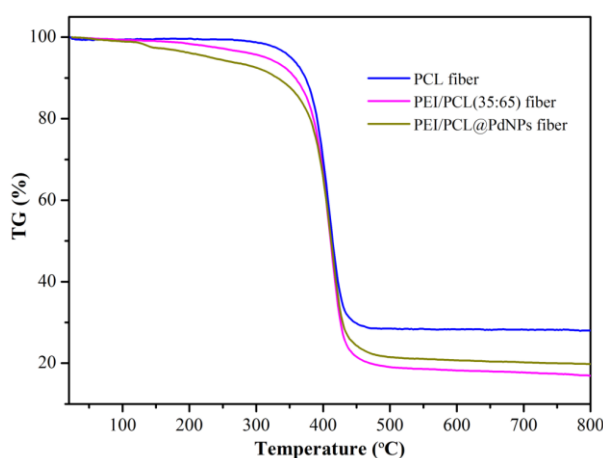


Figure 6. Thermogravimetry (TG) curves of the prepared PCL fibers and PEI/PCL fibers with the weight ratios of 35:65 and PEI/PCL@PdNPs composite.

Next, X-ray photoelectron spectroscopy (XPS) was measured to investigate the interface element composition and the reduction level of Pd^{2+} of the obtained PEI/PCL@PdNPs composite. The results of XPS spectroscopy of PEI/PCL fiber and PEI/PCL@PdNPs composite were shown in Figure 7a. The signals of C1s, N1s and O1s appeared in the XPS full spectrum of PEI/PCL fibers, while the new Pd3d and Si2p signals appeared in the XPS full spectrum of the prepared PEI/PCL@PdNPs. The Si2p signal is due to the contact of the sample with the silicon plate during the examining process. From surface analysis data, the detailed atomic percentages were found to be C = 71.44%, O = 16.08%, N = 6.63%, and Pd = 0.88%. Figure 7b was the deconvolution of the Pd3d peak in the prepared PEI/PCL@PdNPs composite. The XPS spectrum of Pd3d showed double peaks with binding energies at 334.5 eV and 339.7 eV, corresponding to the Pd3d_{5/2} and Pd3d_{3/2} components of the metal Pd(0) state, respectively,

which confirmed the presence of metal Pd [20,42–44]. The above result indicated that excess NaBH_4 reduced all Pd^{2+} in PdCl_2 to Pd^0 without any residual Pd^{2+} ions. The mentioned XPS results further demonstrated the successful preparation of PEI/PCL@PdNPs composites.

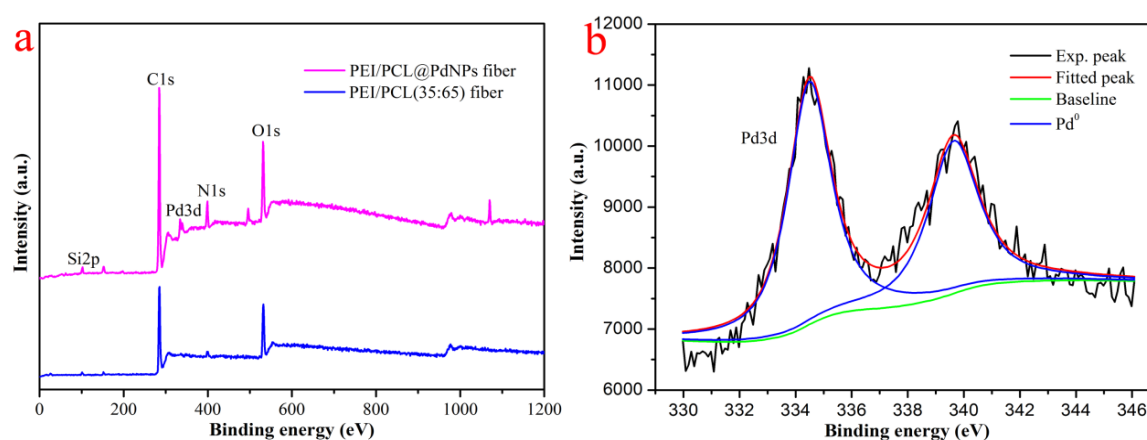


Figure 7. Survey X-ray photoelectron spectroscopy (XPS) spectra of the obtained PEI/PCL fiber and PEI/PCL@PdNPs (a) and deconvolutions of XPS peaks of the Pd3d region (b).

2.2. Catalytic Performance of PEI/PCL@PdNPs Composites

Free palladium nanoparticles exhibit high catalytic activity, while the tendency to aggregate during the catalytic process reduced their catalytic performance. Various palladium composite catalysts reported previously exhibited different catalytic performance at 25 °C, as shown in Table 2 [17–20,45–47]. Therefore, the prepared PEI/PCL@PdNPs composite catalyst was applied to catalytic reduction of 4-NP and 2-NA to explore its catalytic performance. The catalytic activity of PEI/PCL@PdNPs containing active functional groups such as C=O and $-\text{NH}_2$ was attributed to the interaction of PdNPs with the 4-NP substrate adjacent to the catalytic site to promote the reduction of the nitro group. It could be reasonably speculated that the PEI/PCL@PdNPs played a leading role during the catalytic reduction process. When the PEI/PCL@PdNPs catalyst was added to the solution system of the oxidant 4-NP and the reducing agent NaBH_4 , the electrons were transferred from the BH_4^- donor to the 4-NP receptor, thereby producing amino derivative [17]. The 4-nitrophenolate and BH_4^- were adsorbed on the surface of the PEI/PCL@PdNPs catalyst by weak electrostatic interaction. When electrons transferred to Pd NPs, the active hydrogen groups formed and reduced 4-nitrophenol molecules [17]. This electron transfer induced 4-NP hydrogenation spontaneously occurred on the surface of the metal catalyst. Finally, 4-nitroaniline (4-AP) was desorbed from the catalyst surface.

The catalytic performance of PEI/PCL@PdNPs catalyst for 4-NP and 2-NA was observed by UV-visible spectroscopy at room temperature. As shown in Figure 8a, it was clear that the maximum absorption peak at 317 nm of 4-NP aqueous solution shifted to 400 nm owing to the addition of freshly prepared reducing agent NaBH_4 , indicating the formation of 4-nitrophenol ions [48]. At the same time, the color of the mixed solution system changed from light yellow to bright yellow. In addition, 10 mg of PEI/PCL@PdNPs catalyst (PEI:PCL, w/w, 35:65) was added to the system of 4-NP (10 mL, 0.005 M) and NaBH_4 (20 mL, 0.1 M). As shown in Figure 8b, after several seconds, the intensity of the absorption peak at 400 nm significantly decreased and a new absorption peak appeared at 300 nm. Referring to previous literature, the emerging absorption peak corresponded to 4-AP [20]. After 20 seconds, the intensity of the absorption peak at 400 nm of the 4-NP and NaBH_4 mixed system decreased to zero, and the color of the solution became transparent (inset photo in Figure 8b), indicating that all of the 4-NP was reduced to 4-AP. The PEI/PCL@PdNPs catalyst showed high catalytic activity for the reduction of 4-NP, which is attributed to the active sites of PEI/PCL substrate fibers for palladium nanoparticles. In addition, the prepared PEI/PCL@PdNPs composite with weight ratios (w/w, 10:90) catalyst was applied to catalytic reduction of 4-NP to explore its catalytic performance, as shown Figure S1. The

PEI/PCL@PdNPs catalyst at 10:90 weight ratio completely reduced 4-NP to 4-AP in 100 s, and the rate constant k of catalytic reduction reaction was 0.00061 s^{-1} . At the same time, The loading of Pd in the catalyst was found to be Pd = 0.63% in the detailed atomic percentages of PEI/PCL@PdNPs (w/w, 10:90) material. Compared with the PEI/PCL@PdNPs composite at 35:65 weight ratio, it could be reasonably speculated that the improved catalytic performance was owing to more palladium nanoparticles anchored on the surface of PEI/PCL ((w/w), 35:65) fibers with the increment of PEI component in fiber structures. For comparison, the synthesized palladium nanoparticle in solution catalytically reduced the same solution system of 4-NP (10 mL, 0.005 M) and NaBH_4 (20 mL, 0.1 M), and completely reduced 4-NP after 10 minutes, The kinetic constant k of the reduction reaction was 0.006 s^{-1} as shown in Figure S2. The catalytic performance of PEI/PCL@PdNPs catalyst was significantly better than that of palladium nanoparticles in solution, because the PEI/PCL substrate improved the dispersibility of palladium nanoparticles. At the same time, 10 mg of PEI/PCL fibers without Pd nanoparticles was added to the system of 4-NP (10 mL, 0.005 M) and NaBH_4 (20 mL, 0.1 M). After 20 min, no color changes in the solution system had occurred. Moreover, the catalytic properties of PEI/PCL@PdNPs catalyst for the reduction of 2-NA were investigated by the same method. As shown in Figure 8d,e, it was worth mentioning that there was no significant change in the absorption peak of the mixed solution after adding fresh NaBH_4 to the 2-NA solution. After 9 min of addition of the PEI/PCL@PdNPs catalyst, the 2-NA was completely reduced to o-phenylenediamine (OPD), as reported in the literature [49]. The prepared PEI/PCL@PdNPs exhibited different catalytic capabilities for 4-NP and 2-NA. Apparently, PEI/PCL@PdNPs exhibited higher catalytic efficiency for 4-NP. Furthermore, the component amount of palladium nanoparticles on fibers surface depended on the modification times. Compared with appropriate and enough modification time like 1 hour, palladium nanoparticles were hardly found on the surface of PEI/PCL composite fibers at 10 minutes modification with poor catalytic performance.

Table 2. Comparative characteristics and catalytic performance of PdNPs-based materials.

NO.	Materials	Kinetic Constant k/s^{-1}	Characteristics	Refs
1	Pd@B.tea NPs	0.00059	Natural bioactive black tea extract reducing agent	17
2	CN-supported PdNPs nanohybrids	0.00570	Cellulose nanocrystals as support matrix and reducing agent	18
3	AuPdNPs/graphene nanosheets (GNs)	0.01445	Bimetallic nanoparticles, monodisperse method, graphene nanosheet carrier	19
4	nano-silica supported palladium nanocatalyst (Pd/KCC-1)	0.00800	Unique dendritic fibrous morphology led to poor aggregation of PdNPs	20
5	Pd/ magnetic porous carbon (MPC)	0.01200	Porous carbon composite catalyst carrier, magnetic separation	45
6	carbon nanotubes/hyperbranched polymers/Pd (CNT/PiHP/Pd)	0.02630	Carbon nanotube assisted with hyperbranched polymer support	46
7	Pd/Fe ₃ O ₄ @SiO ₂ @KCC-1(silica nanospheres)	0.01960	Core-shell magnetic fibrous nanocatalyst	47
8	Polyethyleneimine(PEI)/Polycaprolactone (PCL)@PdNPs	0.16597	Electrospun fibers carrier, simple method	Present work

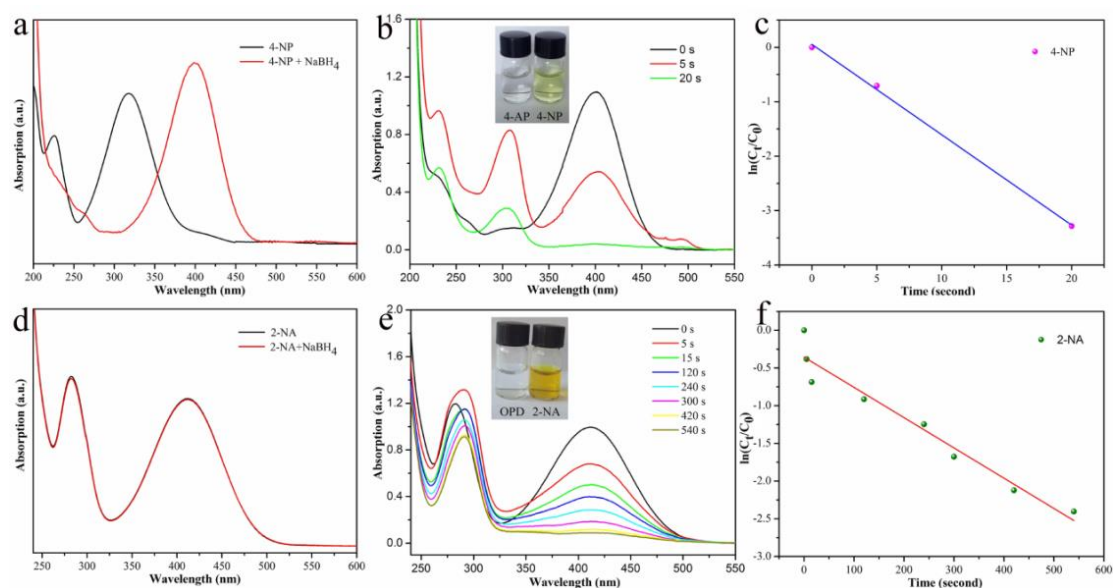


Figure 8. UV absorption curves of 4-NP and 2-NA before and after adding NaBH_4 aqueous solution (a,d); catalytic reduction of 4-NP and 2-NA with PEI/PCL@PdNPs composite (PEI:PCL, w/w, 35:65) and photos of 4-NP and 2-NA solution after reduction (b,e); linear relationship of the reduction process (c,f).

Since the concentration of excess NaBH_4 in the catalytic reaction was much higher than that of 4-NP or 2-NA, the concentration of NaBH_4 in the mixed solution system could be regarded as a constant. Therefore, the concentration of 4-NP or 2-NA was a physical quantity that changed with time t , and the catalytic reduction reaction was a pseudo-first-order reaction [50–57]. The rate of the catalytic reaction (containing adsorption process) was evaluated according to Lambert-Beer's law and pseudo-first-order reaction kinetics (Equation (1)), where A_0 , A_t and C_0 , C_t were the absorbance and concentration of the mixed solution at the initial and time t , respectively. Figure 8c and f were the linear relationships between the reaction time t and $\ln(C_t/C_0)$ of catalytic reduction of 4-NP and 2-NA by PEI/PCL@PdNPs, respectively, reflecting the rate of catalytic reduction of 4-NP and 2-NA by PEI/PCL@PdNPs. The kinetic constant k of the above catalytic reduction reaction was calculated to be 0.16597s^{-1} and 0.00401s^{-1} , respectively. The kinetic constant k could intuitively reflect the speed of the catalytic reduction reaction [58–65]. Obviously, PEI/PCL@PdNPs catalytically reduced 4-NP faster.

$$dC_t/dt = -kt \text{ or } \ln(C_t/C_0) = \ln(A_t/A_0) = -kt \quad (1)$$

The stability and recyclability of the catalyst was another aspect of evaluating the catalyst. Therefore, it was important and necessary to explore the repeated catalytic ability of PEI/PCL@PdNPs catalyst for 4-NP and 2-NA, as shown in Figure 9. The catalytic efficiency of the PEI/PCL@PdNPs catalyst after 8 cycles of repeated catalytic reduction of fresh 4-NP and 2-NA systems were 95% and 92%, respectively. The above result indicated the high catalytic activity, stability and recyclability of the PEI/PCL@PdNPs catalyst. Referring to previous literature, the few decrement in catalytic efficiency was reasonably attributed to the attachment of organics on the surface of catalyst and the loss of palladium particles on the catalyst surface during the washing of PEI/PCL@PdNPs with ethanol and ultrapure water [36].

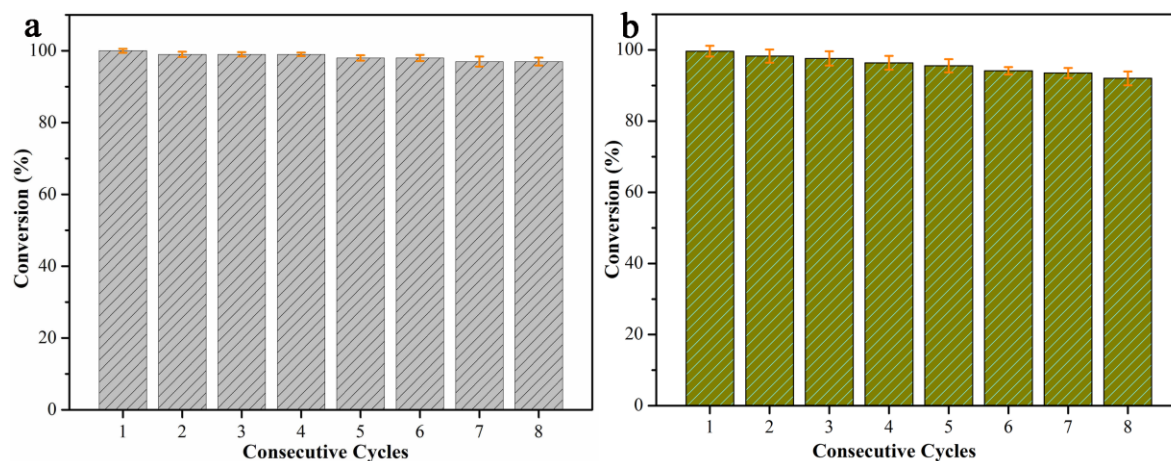


Figure 9. Recyclability test of PEI/PCL@PdNPs catalyst for the reduction of 4-NP (a) and 2-NA (b).

3. Materials and Methods

3.1. Materials

Polyethylenimine (PEI, M.W. 600.99%) was purchased from Shanghai Aladdin Biochemical Technology Co., Ltd. (Shanghai, China), and the same with Palladium chloride (PdCl₂, Pd 59–60%). Polycaprolactone (PCL, average Mn 80,000) was obtained from Sigma-Aldrich (Shanghai) Trading Co. Ltd. (China). Trichloromethane (CHCl₃) was obtained from Jindong Tianzheng Co. Ltd. In addition, Sodium borohydride (NaBH₄), 2-nitroaniline (2-NA) and 4-nitrophenol (4-NP) were obtained from Alfa Aesar (Beijing, China). All chemicals were not further purified. A Milli-Q Millipore Filtration System (Millipore Co., Bedford, MA, USA) was used to prepare ultrapure water.

3.2. Preparation of PEI/PCL@PdNPs Composites

11% (w/v) polycaprolactone polymer solution was prepared by dissolving PCL in chloroform referring to previous literature [66,67]. Secondly, according to the different blend ratios of PEI:PCL (10:90, 15:85, 20:80, 25:75, 30:70, 35:65 (w/w)), PEI were added to the abovementioned 11% polycaprolactone solution to obtain different concentration gradients of PEI/PCL mixed solutions. The PEI/PCL mixed solutions of different blend ratios were magnetically stirred overnight at room temperature to obtain uniform electrospinning precursor solutions. The precursor solutions were sequentially electrospun under the parameters of 15 kV voltage, 1 mL/h flow rate, and 25 cm distance between the needle and the receiving plate to obtain PEI/PCL electrospun composite fibers (samples 1–6) of different blend ratios.

0.003 M PdCl₂ aqueous solution and 0.01 M NaBH₄ solution were disposed in 50 mL volumetric bottles respectively. The above-mentioned PdCl₂ aqueous solution (20 mL) in a clean beaker was stirred vigorously and subsequently added 0.01 M NaBH₄ solution drop by drop until the color of the solution changed from khaki to dark brown, indicating the reduction of Pd²⁺ to Pd⁰ and the formation of Pd particles [68]. Then two species of 10 mg PEI/PCL composite fibers (sample 1 and 6) were added to the above-mentioned Pd particles solution and continued stirring vigorously to avoid the Pd particles agglomeration. After an hour, the PEI/PCL fibers were taken out and washed with deionized water three times before drying. Thus, the PEI/PCL@PdNPs composite materials (sample 7 and 8) were obtained and completed the chemical modification of Pd particles.

3.3. Catalytic Performance of PEI/PCL@PdNPs Composite

According to the previous literature, the prepared PEI/PCL@PdNPs composite was used as a catalyst to reduce 4-NP and 2-NA. The entire catalytic experiment was carried out at 25 °C. Fresh NaBH₄ solution (20 mL, 0.1 M) was thoroughly mixed with 4-NP solution (10 mL, 0.005 M), and the

UV–vis spectrum of the mixed solution was measured as the absorbance value at the initial time (0 s). Subsequently, 10 mg of the prepared PEI/PCL@PdNPs composite was quickly added to the mixed solution. The absorbance of the mixed solution was measured by UV–vis spectroscopy at intervals (5 s, 15 s, 20 s) until it was reduced to zero, and the catalytic curve of PEI/PCL@PdNPs catalyst for 4-NP was obtained. The same method was used to investigate the catalytic performance of PEI/PCL@PdNPs catalyst for 2-NA solution. NaBH₄ acted as a reducing agent during the catalytic reduction process. At the same time, according to the above experimental method, PEI/PCL@PdNPs catalyst was carried out repeated catalytic experiments on fresh 4-NP and NaBH₄ mixed solutions. After the catalytic reduction reaction is completed, the PEI/PCL@PdNPs catalyst was removed and the washed several times with ethanol and ultrapure water until the color of the washing liquid did not change. The washed PEI/PCL@PdNPs were then dried for the next catalytic experiment. Catalytic reduction of fresh 4-NP and 2-NA solutions was carried out 8 times in succession.

3.4. Characterization

Scanning electron microscope (SEM, FEI Corporate, Hillsboro, OR, USA) with a field emission gun FEI QUANTA FEG 250 were measured to obtain the morphologies of prepared electrospun fibers. Before measurement, the samples were coated with AuNPs by sputtering in vacuum for 30 seconds. In addition, energy dispersive spectroscopy (EDS) were utilized to acquire the chemical elements analysis of the as-obtained fiber samples. The morphology of the samples was further characterized via Transmission electron microscopy (TEM, HT7700, High-Technologies Corp., Ibaraki, Japan). The microstructure was observed by High-resolution transmission electron microscopy (HRTEM, Tecnai-G2 F30 S-TWIN, Philips, Netherlands). X-ray diffraction patterns were conducted on an X-ray diffractometer (SMART LAB, Rigaku, Akishima, Japan) with a CuK α X-ray radiation source and a Bragg diffraction apparatus. Thermogravimetry-differential scanning calorimetry (TG-DSC) analysis was carried out by NETZSCH STA 409 PC Luxxi thermal analyzer (Netzsch Instruments Manufacturing Co., Ltd., Seligenstadt, Germany) under argon gas atmosphere. X-ray photoelectron spectroscopy (XPS) was investigated on Thermo Scientific ESCALab 250Xi (Netzsch Instrument Manufacturing GmbH, Seligenstadt, Germany) equipped with 200 W of monochromatic AlK α radiation. UV-vis absorption spectra were measured with UV-visible spectroscopy (UV-2550, Shimadzu Corporation, Tokyo, Japan). BET measurements (NOVA 4200-P, Quantachrome Instruments, Boynton Beach, FL, USA) were obtained to characterize the specific surface areas and pore diameter distribution. The surface areas were calculated by the Brunauer–Emmett–Teller (BET) method.

4. Conclusions

In summary, we have successfully designed and prepared PEI/PCL@PdNPs composite fiber catalyst with remarkable catalytic activity and stability. After the microscopic morphology of the PEI/PCL fibers was regulated, the plenty of pits structures appeared on the surface of the fibers increased the specific surface area of solid substrate fibers and provided abundant active attachment sites and sufficient space for the chemical modification of the palladium nanoparticles, which favored the adhesion of the palladium particles. The catalytic reduction of 4-nitrophenol and 2-nitroaniline by PEI/PCL@PdNPs catalyst exhibited fast, stable and reusable catalytic performance. This work provided new research clues for the preparation of composites loaded with PdNPs and ideal metal particle-based carriers.

Supplementary Materials: The following are available online at <http://www.mdpi.com/2073-4344/9/6/559/s1>, Figure S1. UV–vis absorption curves of catalytic reduction of 4-NP with (PEI:PCL, w/w, 10:90) PEI/PCL@PdNPs composite (a) and linear relationship of the reduction process (b). Figure S2. UV–vis absorption curves of catalytic reduction of 4-NP via PdNPs solution (a), PEI/PCL fibers (b), and linear relationship of the reduction process (c).

Author Contributions: T.J. and Q.P. conceived and designed the experiments; C.W. and J.Y. performed the experiments; S.H., J.Z., and L.Z. analyzed the data; Z.B. and Q.P. contributed reagents/materials/analysis tools; C.W. and T.J. wrote the paper.

Funding: This research was funded by the National Natural Science Foundation of China (No. 21872119), the Support Program for the Top Young Talents of Hebei Province, China Postdoctoral Science Foundation (No. 2015M580214), and the Research Program of the College Science & Technology of Hebei Province (No. ZD2018091).

Conflicts of Interest: The authors declare no conflict of interest.

References

1. Amezcua-García, H.J.; Razo-Flores, E.; Cervantes, F.J.; Rangel-Mendez, J.R. Activated carbon fibers as redox mediators for the increased reduction of nitroaromatics. *Carbon* **2013**, *55*, 276–284. [[CrossRef](#)]
2. El-Sheikh, S.M.; Ismail, A.A.; Al-Sharab, J.F. Catalytic reduction of p-nitrophenol over precious metals/highly ordered mesoporous silica. *New J. Chem.* **2013**, *37*, 2399–2407. [[CrossRef](#)]
3. Dieckmann, M.S.; Gray, K.A. A comparison of the degradation of 4-nitrophenol via direct and sensitized photocatalysis in TiO₂ slurries. *Water Res.* **1996**, *30*, 1169–1183. [[CrossRef](#)]
4. Marais, E.; Nyokong, T. Adsorption of 4-nitrophenol onto Amberlite®IRA-900 modified with metallophthalocyanines. *J. Hazard. Mater.* **2008**, *152*, 293–301. [[CrossRef](#)]
5. Liu, N.; Li, H.; Ding, F.; Xiu, Z.; Liu, P.; Yu, Y. Analysis of biodegradation by-products of nitrobenzene and aniline mixture by a cold-tolerant microbial consortium. *J. Hazard. Mater.* **2013**, *260*, 323–329. [[CrossRef](#)] [[PubMed](#)]
6. Zhang, L.; Zheng, S.; Kang, D.E.; Shin, J.Y.; Suh, H.; Kim, I. Synthesis of multi-amine functionalized hydrogel for preparation of noble metal nanoparticles: Utilization as highly active and recyclable catalysts in reduction of nitroaromatics. *RSC Adv.* **2013**, *3*, 4692–4703. [[CrossRef](#)]
7. Boothroyd, S.R.; Kerr, M.A. A mild and efficient method for the preparation of anilines from nitroarenes. *Tetrahedron Lett.* **1995**, *36*, 2411–2414. [[CrossRef](#)]
8. Pérez-Lorenzo, M. Palladium nanoparticles as efficient catalysts for Suzuki cross-coupling reactions. *J. Phys. Chem. Lett.* **2012**, *3*, 167–174. [[CrossRef](#)]
9. Hildebrand, H.; Mackenzie, K.; Kopinke, F.D. Highly active Pd-on-magnetite nanocatalysts for aqueous phase hydrodechlorination reactions. *Environ. Sci. Technol.* **2009**, *43*, 3254–3259. [[CrossRef](#)]
10. Esumi, K.; Isono, R.; Yoshimura, T. Preparation of PAMAM- and PPI-Metal (silver, platinum, and palladium) nanocomposites and their catalytic activities for reduction of 4-nitrophenol. *Langmuir* **2004**, *20*, 237–243. [[CrossRef](#)]
11. Lin, Y.; Qiao, Y.; Wang, Y.; Yan, Y.; Huang, J. Self-assembled laminated nanoribbon-directed synthesis of noble metallic nanoparticle-decorated silica nanotubes and their catalytic applications. *J. Mater. Chem.* **2012**, *22*, 18314–18320. [[CrossRef](#)]
12. Oka, S.; Kamegawa, T.; Mori, K.; Yamashita, H. An electroless deposition technique for the synthesis of highly active and nano-sized Pd particles on silica nanosphere. *Catal. Today* **2012**, *185*, 109–112. [[CrossRef](#)]
13. Li, Y.; Fan, X.; Qi, J.; Ji, J.; Wang, S.; Zhang, G.; Zhang, F. Palladium nanoparticle-graphene hybrids as active catalysts for the Suzuki reaction. *Nano Res.* **2010**, *3*, 429–437. [[CrossRef](#)]
14. Hermans, S.; Bruyr, V.; Devillers, M. A templating effect of carbon nanomaterials on the synthesis of Pd nanoparticles by covalent grafting onto surface O-groups. *J. Mater. Chem.* **2012**, *22*, 14479–14486. [[CrossRef](#)]
15. Liu, J.; Li, Y.Q.; Zheng, W.J. Synthesis of immobilized nanopalladium on polymer-supported Schiff base, and study of its catalytic activity in the Suzuki–Miyaura reaction. *Monatsh. Chem.* **2009**, *140*, 1425. [[CrossRef](#)]
16. Domènech, B.; Muñoz, M.; Muraviev, D.N.; Macanás, J. Polymer-stabilized palladium nanoparticles for catalytic membranes: Ad hoc polymer fabrication. *Nanoscale Res. Lett.* **2011**, *6*, 406. [[CrossRef](#)]
17. Lebaschi, S.; Hekmati, M.; Veisi, H. Green synthesis of palladium nanoparticles mediated by black tea leaves (*Camellia sinensis*) extract: Catalytic activity in the reduction of 4-nitrophenol and Suzuki–Miyaura coupling reaction under ligand-free conditions. *J. Colloid Interf. Sci.* **2017**, *485*, 223–231. [[CrossRef](#)]
18. Wu, X.; Lu, C.; Zhang, W.; Yuan, G.; Xiong, R.; Zhang, X. A novel reagentless approach for synthesizing cellulose nanocrystal-supported palladium nanoparticles with enhanced catalytic performance. *J. Mater. Chem. A* **2013**, *1*, 8645–8652. [[CrossRef](#)]
19. Chen, X.; Cai, Z.; Chen, X.; Oyama, M. AuPd bimetallic nanoparticles decorated on graphene nanosheets: Their green synthesis, growth mechanism and high catalytic ability in 4-nitrophenol reduction. *J. Mater. Chem. A* **2014**, *2*, 5668–5674. [[CrossRef](#)]

20. Le, X.; Dong, Z.; Li, X.; Zhang, W.; Le, M.; Ma, J. Fibrous nano-silica supported palladium nanoparticles: An efficient catalyst for the reduction of 4-nitrophenol and hydrodechlorination of 4-chlorophenol under mild conditions. *Catal. Commun.* **2015**, *59*, 21–25. [[CrossRef](#)]
21. Bhardwaj, N.; Kundu, S.C. Electrospinning: A fascinating fiber fabrication technique. *Biotechnol. Adv.* **2010**, *28*, 325–347. [[CrossRef](#)] [[PubMed](#)]
22. Huang, Z.M.; Zhang, Y.Z.; Kotaki, M.; Ramakrishna, S. A review on polymer nanofibers by electrospinning and their applications in nanocomposites. *Compos. Sci. Technol.* **2003**, *63*, 2223–2253. [[CrossRef](#)]
23. Shariful, M.I.; Sharif, S.B.; Lee, J.J.L.; Habiba, U.; Ang, B.C.; Amalina, M.A. Adsorption of divalent heavy metal ion by mesoporous-high surface area chitosan/poly (ethylene oxide) nanofibrous membrane. *Carbohydr. Polym.* **2017**, *157*, 57–64. [[CrossRef](#)] [[PubMed](#)]
24. Su, C.; Li, Y.; Dai, Y.; Gao, F.; Tang, K.; Cao, H. Fabrication of three-dimensional superhydrophobic membranes with high porosity via simultaneous electrospinning and electrospinning. *Mater. Lett.* **2016**, *170*, 67–71. [[CrossRef](#)]
25. Habiba, U.; Afifi, A.M.; Salleh, A.; Ang, B.C. Chitosan/(polyvinyl alcohol)/zeolite electrospun composite nanofibrous membrane for adsorption of Cr^{6+} , Fe^{3+} and Ni^{2+} . *J. Hazard. Mater.* **2017**, *322*, 182–194. [[CrossRef](#)] [[PubMed](#)]
26. Zhao, R.; Wang, Y.; Li, X.; Sun, B.; Wang, C. Synthesis of β -cyclodextrin-based electrospun nanofiber membranes for highly efficient adsorption and separation of methylene blue. *ACS Appl. Mater. Inter.* **2015**, *7*, 26649–26657. [[CrossRef](#)] [[PubMed](#)]
27. Shang, C.; Li, M.; Wang, Z.; Wu, S.; Lu, Z. Electrospun nitrogen-doped carbon nanofibers encapsulating cobalt nanoparticles as efficient oxygen reduction reaction catalysts. *ChemElectroChem* **2016**, *3*, 1437–1445. [[CrossRef](#)]
28. Ye, J.S.; Liu, Z.T.; Lai, C.C.; Lo, C.T.; Lee, C.L. Diameter effect of electrospun carbon fiber support for the catalysis of Pt nanoparticles in glucose oxidation. *Chem. Eng. J.* **2016**, *283*, 304–312. [[CrossRef](#)]
29. Zhu, M.M.; Han, J.Q.; Wang, F.; Shao, W.; Xiong, R.H.; Zhang, Q.L.; Pan, H.; Yang, Y.; Samal, S.K.; Zhang, F.; et al. Electrospun nanofibers membranes for effective air filtration. *Macromol. Mater. Eng.* **2017**, *302*, 1600353. [[CrossRef](#)]
30. Jiang, S.; Hou, H.; Agarwal, S.; Greiner, A. Polyimide nanofibers by “Green” electrospinning via aqueous solution for filtration applications. *ACS Sustain. Chem. Eng.* **2016**, *4*, 4797–4804. [[CrossRef](#)]
31. Yoshimoto, H.; Shin, Y.M.; Terai, H.; Vacanti, J.P. A biodegradable nanofiber scaffold by electrospinning and its potential for bone tissue engineering. *Biomaterials* **2003**, *24*, 2077–2082. [[CrossRef](#)]
32. Xu, T.; Liang, Z.; Ding, B.; Feng, Q.; Fong, H. Polymer blend nanofibers containing polycaprolactone as biocompatible and biodegradable binding agent to fabricate electrospun three-dimensional scaffolds/structures. *Polymer* **2018**, *151*, 299–306. [[CrossRef](#)]
33. Baker, S.R.; Banerjee, S.; Bonin, K.; Guthold, M. Determining the mechanical properties of electrospun poly- ϵ -caprolactone (PCL) nanofibers using AFM and a novel fiber anchoring technique. *Mater. Sci. Eng. C* **2016**, *59*, 203–212. [[CrossRef](#)] [[PubMed](#)]
34. Delyanee, M.; Solouk, A.; Akbari, S.; Seyedjafari, E. Modification of electrospun poly(L-lactic acid)/polyethylenimine nanofibrous scaffolds for biomedical application. *Inter. J. Polym. Mater.* **2018**, *67*, 247–257. [[CrossRef](#)]
35. Guo, Y.; Xu, Y.T.; Gao, G.H.; Wang, T.; Zhao, B.; Fu, X.Z.; Sun, R.; Wong, C.P. Electro-oxidation of formaldehyde and methanol over hollow porous palladium nanoparticles with enhanced catalytic activity. *Catal. Commun.* **2015**, *58*, 40–45. [[CrossRef](#)]
36. Guo, R.; Jiao, T.F.; Xing, R.R.; Chen, Y.; Guo, W.C.; Zhou, J.X.; Zhang, L.X.; Peng, Q.M. Hierarchical AuNPs-loaded Fe_3O_4 /polymers nanocomposites constructed by electrospinning with enhanced and magnetically recyclable catalytic capacities. *Nanomaterials* **2017**, *7*, 317. [[CrossRef](#)]
37. Zhang, Y.W.; Peng, H.H.; Huang, W.; Zhou, Y.F.; Zhang, X.H.; Yan, D.Y. Hyperbranched poly (amidoamine) as the stabilizer and reductant to prepare colloid silver nanoparticles in situ and their antibacterial activity. *J. Phys. Chem. C* **2008**, *112*, 2330–2336. [[CrossRef](#)]
38. Li, C.L.; Su, Y.; Lv, X.Y.; Shi, H.J.; Yang, X.G.; Wang, Y.J. Enhanced ethanol electrooxidation of hollow Pd nanospheres prepared by galvanic exchange reactions. *Mater. Lett.* **2012**, *69*, 92–95. [[CrossRef](#)]

39. Yang, L.; Hu, C.G.; Wang, J.L.; Yang, Z.X.; Guo, Y.M.; Bai, Z.Y.; Wang, K. Facile synthesis of hollow palladium/copper alloyed nanocubes for formic acid oxidation. *Chem. Commun.* **2011**, *47*, 8581–8583. [[CrossRef](#)]
40. Ji, Y.; Ghosh, K.; Shu, X.Z.; Li, B.Q.; Sokolov, J.C.; Prestwich, G.D.; Clark, R.A.F.; Rafailovich, M.H. Electrospun three-dimensional hyaluronic acid nanofibrous scaffolds. *Biomaterials* **2006**, *27*, 3782–3792. [[CrossRef](#)]
41. Konwer, S.; Boruah, R.; Dolui, S.K. Studies on conducting polypyrrole/graphene oxide composites as supercapacitor electrode. *J. Electron. Mater.* **2011**, *40*, 2248. [[CrossRef](#)]
42. Yang, S.D.; Dong, J.; Yao, Z.H.; Shen, C.M.; Shi, X.Z.; Tian, Y.; Lin, S.X.; Zhang, X.G. One-pot synthesis of graphene-supported monodisperse Pd nanoparticles as catalyst for formic acid electro-oxidation. *Sci. Rep.* **2014**, *4*, 4501. [[CrossRef](#)] [[PubMed](#)]
43. Zhu, Q.L.; Song, F.Z.; Wang, Q.J.; Tsumori, N.; Himeda, Y.; Autrey, T.; Xu, Q. A solvent-switched in situ confinement approach for immobilizing highly-active ultrafine palladium nanoparticles: Boosting catalytic hydrogen evolution. *J. Mater. Chem. A* **2018**, *6*, 5544–5549. [[CrossRef](#)]
44. Jin, Z.; Nackashi, D.; Lu, W.; Kittrell, C.; Tour, J.M. Decoration, migration, and aggregation of palladium nanoparticles on graphene sheets. *Chem. Mater.* **2010**, *22*, 5695–5699. [[CrossRef](#)]
45. Dong, Z.P.; Le, X.D.; Liu, Y.S.; Dong, C.X.; Ma, J.T. Metal organic framework derived magnetic porous carbon composite supported gold and palladium nanoparticles as highly efficient and recyclable catalysts for reduction of 4-nitrophenol and hydrodechlorination of 4-chlorophenol. *J. Mater. Chem. A* **2014**, *2*, 18775–18785. [[CrossRef](#)]
46. Li, H.; Han, L.; Cooper-White, J.; Kim, I. Palladium nanoparticles decorated carbon nanotubes: Facile synthesis and their applications as highly efficient catalysts for the reduction of 4-nitrophenol. *Green Chem.* **2012**, *14*, 586–591. [[CrossRef](#)]
47. Le, X.; Dong, Z.; Liu, Y.; Jin, Z.; Huy, T.D.; Le, M.; Ma, J. Palladium nanoparticles immobilized on core-shell magnetic fibers as a highly efficient and recyclable heterogeneous catalyst for the reduction of 4-nitrophenol and Suzuki coupling reactions. *J. Mater. Chem. A* **2014**, *2*, 19696–19706. [[CrossRef](#)]
48. Kim, K.; Kim, K.L.; Shin, K.S. Co-reduced Ag/Pd bimetallic nanoparticles: Surface enrichment of Pd revealed by Raman spectroscopy. *J. Phys. Chem. C* **2011**, *115*, 14844–14851. [[CrossRef](#)]
49. Abay, A.K.; Kuo, D.H.; Chen, X.; Saragih, A.D. A new V-doped Bi₂(O,S)₃ oxysulfide catalyst for highly efficient catalytic reduction of 2-nitroaniline and organic dyes. *Chemosphere* **2017**, *189*, 21–31. [[CrossRef](#)]
50. Jana, S.; Ghosh, S.K.; Nath, S.; Pande, S.; Praharaj, S.; Panigrahi, S.; Basu, S.; Endo, T.; Pal, T. Synthesis of silver nanoshell-coated cationic polystyrene beads: A solid phase catalyst for the reduction of 4-nitrophenol. *Appl. Catal. A-Gen.* **2006**, *313*, 41–48. [[CrossRef](#)]
51. Jiao, T.F.; Zhao, H.; Zhou, J.X.; Zhang, Q.R.; Luo, X.N.; Hu, J.; Peng, Q.M.; Yan, X.H. Self-Assembly Reduced Graphene Oxide Nanosheet Hydrogel Fabrication by Anchorage of Chitosan/Silver and Its Potential Efficient Application toward Dyes Degradation for Wastewater Treatments. *ACS Sustain. Chem. Eng.* **2015**, *3*, 3130–3139. [[CrossRef](#)]
52. Guo, R.; Jiao, T.F.; Li, R.F.; Chen, Y.; Guo, W.C.; Zhang, L.X.; Zhou, J.X.; Zhang, Q.R.; Peng, Q.M. Sandwiched Fe₃O₄/carboxylate graphene oxide nanostructures constructed by layer-by-layer assembly for highly efficient and magnetically recyclable dye removal. *ACS Sustain. Chem. Eng.* **2018**, *6*, 1279–1288. [[CrossRef](#)]
53. Wang, C.R.; Sun, S.X.; Zhang, L.X.; Yin, J.J.; Jiao, T.F.; Zhang, L.; Xu, Y.L.; Zhou, J.X.; Peng, Q.M. Facile preparation and catalytic performance characterization of AuNPs-loaded hierarchical electrospun composite fibers by solvent vapor annealing treatment. *Colloid Surf. A* **2019**, *561*, 283–291. [[CrossRef](#)]
54. He, Y.; Wang, R.; Jiao, T.F.; Yan, X.Y.; Wang, M.L.; Zhang, L.X.; Bai, Z.H.; Zhang, Q.; Peng, Q.M. Facile Preparation of Self-Assembled Layered Double Hydroxide-Based Composite Dye Films as New Chemical Gas Sensors. *ACS Sustain. Chem. Eng.* **2019**, *7*, 10888–10899. [[CrossRef](#)]
55. Feng, Y.; Jiao, T.F.; Yin, J.J.; Zhang, L.; Zhang, L.X.; Zhou, J.X.; Peng, Q.M. Facile Preparation of Carbon Nanotube-Cu₂O Nanocomposites as New Catalyst Materials for Reduction of p-Nitrophenol. *Nanoscale Res. Lett.* **2019**, *14*, 78. [[CrossRef](#)]
56. Chen, K.Y.; Jiao, T.F.; Li, J.K.; Han, D.X.; Wang, R.; Tian, G.J.; Peng, Q.M. Chiral Nanostructured Composite Films via Solvent-Tuned Self-Assembly and Their Enantioselective Performances. *Langmuir* **2019**, *35*, 3337–3345. [[CrossRef](#)] [[PubMed](#)]

57. Chen, K.Y.; Yan, X.Y.; Li, J.K.; Jiao, T.F.; Cai, C.; Zou, G.D.; Wang, R.; Wang, M.L.; Zhang, L.X.; Peng, Q.M. Preparation of Self-Assembled Composite Films Constructed by Chemically-Modified MXene and Dyes with Surface-enhanced Raman Scattering Characterization. *Nanomaterials* **2019**, *9*, 284. [[CrossRef](#)]
58. Sun, S.X.; Wang, C.R.; Han, S.Q.; Jiao, T.F.; Wang, R.; Yin, J.J.; Li, Q.; Wang, Y.Q.; Geng, L.J.; Yu, X.D.; et al. Interfacial nanostructures and acidochromism behaviors in self-assembled terpyridine derivatives Langmuir-Blodgett films. *Colloid Surf. A* **2019**, *564*, 1–9. [[CrossRef](#)]
59. Huang, X.X.; Jiao, T.F.; Liu, Q.Q.; Zhang, L.X.; Zhou, J.X.; Li, B.B.; Peng, Q.M. Hierarchical electrospun nanofibers treated by solvent vapor annealing as air filtration mat for high-efficiency PM2.5 capture. *Sci. China Mater.* **2019**, *62*, 423–436. [[CrossRef](#)]
60. Wang, C.R.; Yin, J.J.; Wang, R.; Jiao, T.F.; Huang, H.M.; Zhou, J.X.; Zhang, L.X.; Peng, Q.M. Facile preparation of self-assembled polydopamine-modified electrospun fibers for highly effective removal of organic dyes. *Nanomaterials* **2019**, *9*, 116. [[CrossRef](#)]
61. Guo, R.; Wang, R.; Yin, J.J.; Jiao, T.F.; Huang, H.M.; Zhao, X.M.; Zhang, L.X.; Li, Q.; Zhou, J.X.; Peng, Q.M. Fabrication and highly efficient dye removal characterization of beta-cyclodextrin-based composite polymer fibers by electrospinning. *Nanomaterials* **2019**, *9*, 127. [[CrossRef](#)] [[PubMed](#)]
62. Huang, X.X.; Wang, R.; Jiao, T.F.; Zou, G.D.; Zhan, F.K.; Yin, J.J.; Zhang, L.X.; Zhou, J.X.; Peng, Q.M. Facile Preparation of Hierarchical AgNP-Loaded MXene/Fe₃O₄/Polymer Nanocomposites by Electrospinning with Enhanced Catalytic Performance for Wastewater Treatment. *ACS Omega* **2019**, *4*, 1897–1906. [[CrossRef](#)]
63. Yin, Y.R.; Ma, N.; Xue, J.; Wang, G.Q.; Liu, S.B.; Li, H.L.; Guo, P.Z. Insights into the Role of Poly(vinylpyrrolidone) in the Synthesis of Palladium Nanoparticles and Their Electrocatalytic Properties. *Langmuir* **2019**, *35*, 787–795. [[CrossRef](#)] [[PubMed](#)]
64. Liu, K.; Yuan, C.Q.; Zou, Q.L.; Xie, Z.C.; Yan, X.H. Self-Assembled Zinc/Cystine-Based Chloroplast Mimics Capable of Photoenzymatic Reactions for Sustainable Fuel Synthesis. *Angew. Chem. Int. Ed.* **2017**, *56*, 7876–7880. [[CrossRef](#)] [[PubMed](#)]
65. Yan, X.Y.; Wang, M.L.; Sun, X.; Wang, Y.H.; Shi, G.H.; Ma, W.L.; Hou, P. Sandwich-like Ag@Cu@CW SERS substrate with tunable nanogaps and component based on the Plasmonic nanonodule structures for sensitive detection crystal violet and 4-aminothiophenol. *Appl. Surf. Sci.* **2019**, *479*, 879–886. [[CrossRef](#)]
66. Ma, K.; Chen, W.; Jiao, T.; Jin, X.; Sang, Y.; Yang, D.; Zhou, J.; Liu, M.; Duan, P. Boosting Circularly Polarized Luminescence of Small Organic Molecules via Multi-dimensional Morphology Control. *Chem. Sci.* **2019**. [[CrossRef](#)]
67. Liu, J.Z.; Bauer, A.J.P.; Li, B.B. Solvent vapor annealing: An efficient approach for inscribing secondary nanostructures onto electrospun fibers. *Macromol. Rapid Comm.* **2014**, *35*, 1503–1508. [[CrossRef](#)]
68. Nasrollahzadeh, M.; Sajadi, S.M.; Honarmand, E.; Maham, M. Preparation of palladium nanoparticles using Euphorbia thymifolia L. leaf extract and evaluation of catalytic activity in the ligand-free Stille and Hiyama cross-coupling reactions in water. *New J. Chem.* **2015**, *39*, 4745–4752. [[CrossRef](#)]

